

Extreme pulse-front tilt from an etalon

Pamela Bowlan^{1,2,*} and Rick Trebino^{1,2}

¹Swamp Optics, LLC, 6300 Powers Ferry Road No. 600-345, Atlanta, Georgia 30339-2919, USA

²Georgia Institute of Technology, School of Physics, 837 State Street, Atlanta, Georgia 30332-0430, USA

*Corresponding author: pambowlan@gatech.edu

Received June 14, 2010; revised July 18, 2010; accepted July 19, 2010;
posted August 19, 2010 (Doc. ID 130066); published October 18, 2010

Angular dispersion—whether from prisms, diffraction gratings, or etalons—is well known to result in a pulse-front tilt. Focusing into a tilted etalon, in particular, generates a huge angular dispersion, which is very useful for high-resolution spectrometers and pulse shapers. Here we demonstrate experimentally that, due to the large angular dispersion ($\sim 3^\circ/\text{nm}$), the pulse directly out of an etalon can have a huge pulse-front tilt— 89.9° —which can cause one side of a few-millimeter-wide beam to lead the other by 1 m, that is, several nanoseconds. We propagated a 700 ps near-transform-limited pulse through the etalon and measured the resulting spatiotemporal field, confirming this result. To make this measurement, we used a high-spectral-resolution version of crossed-beam spectral interferometry, which used a high-resolution etalon spectrometer. We also performed simulations, which we found to be in good agreement with our measurements. © 2010 Optical Society of America

OCIS codes: 320.5550, 300.6190, 320.7100, 320.4240.

1. INTRODUCTION

It is well known that the spatial and temporal dependencies of the electric fields of light pulses, especially femtosecond pulses, are often coupled and so cannot be assumed to be independent [1]. This is because common optical elements can introduce *spatiotemporal couplings* or cross dependencies in space x and time t in the light pulse's electric field.

Because the electric field $E(x, t)$ of the pulse can be represented equivalently in any Fourier domain, xt , $x\omega$, $k_x\omega$, or $k_x t$, a given spatiotemporal coupling actually manifests itself as several seemingly different, but in fact equivalent, effects when viewed in any of the other domains [1]. Indeed, a common spatiotemporal coupling is *angular dispersion*, which is a cross term in the intensity (real) of the field $E(k_x, \omega)$,

$$\hat{E}(k_x, \omega) = \hat{E}_0[k_x + \gamma(\omega - \omega_0), \omega], \quad (1)$$

where γ is the coupling constant, and ω_0 is the pulse center frequency; the overtilde means Fourier transformation from the time domain t to the frequency domain ω , and the hat (\wedge) indicates Fourier transformation from x to k_x . By simply Fourier transforming to the xt -domain (and applying the shift and then inverse shift theorems), it is easy to see that, if angular dispersion is present, there is always a corresponding xt coupling in the intensity, known as the *pulse-front tilt* (PFT) [2–6]:

$$E(x, t) \propto E_0(x, t + \gamma x). \quad (2)$$

It is interesting that angular dispersion is, however, not the only source of the PFT [1,7]. There is an additional contribution to the PFT due to the simultaneous presence of temporal and spatial chirps. For Gaussian beams and pulses, the following analytical relationship between angular dispersion and PFT can be found:

$$\text{PFT} = k_0\beta + \varphi^{(2)}v, \quad (3)$$

where $k_0 = 2\pi/\lambda_0$, β is the angular dispersion, v is the spatial chirp, and $\varphi^{(2)}$ is the temporal chirp due to group delay dispersion [1,7].

In the absence of spatial or temporal chirp, however, the PFT is linearly proportional to the angular dispersion—*independent of the cause of the angular dispersion*—so, because diffraction gratings generally introduce more angular dispersion than prisms, they also yield a more tilted pulse front. The PFT from diffraction gratings and prisms has been investigated in detail and even put to a good use. For example, PFT has been used to make single-shot autocorrelation measurements of many-picosecond pulses [8,9]. The PFT has also been useful for micromachining [10].

Bor *et al.* pointed out that less commonly used sources of dispersion, such as etalons [3], also introduce PFTs. This was also observed and used for time domain pulse shaping by Xiao *et al.* [11]; and because the angular dispersion introduced by an etalon can be orders of magnitude more than that of prisms and gratings, their PFTs can be extremely large. This is the phenomenon that we investigate in this paper.

An etalon is simply two parallel highly reflecting surfaces, in which the output beam is the superposition of many delayed replicas of the input beam. The delay between each replica is $2nd/c$, where $2d$ is the etalon round-trip length, and n is the refractive index of the medium inside the etalon. Due to the interference of the many output beams, only colors having a wavelength that is an integer (m) multiple of the etalon's width, or $m\lambda_0/n = 2d$, exit the cavity without loss. Therefore, when focusing into an etalon, a range of path lengths is present, one for each ray, so different colors will exit the cavity along different

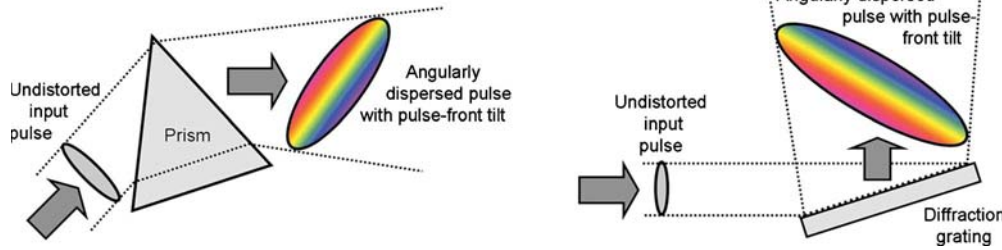


Fig. 1. (Color online) Prisms and diffraction gratings introduce angular dispersion or, if viewed in time, PFT. In prisms, the group delay is greater for rays that pass through the base of the prism than those that pass through the tip. In gratings, rays that impinge on the near edge of the grating emerge sooner and so precede those that must travel all the way to the far edge of the grating. While the reasons for the PFT are seemingly unrelated, the PFT can be shown to be due to the angular dispersion of the component.

rays, or angles, resulting in its well-known angular dispersion [12].

For a given beam size, etalons can be used to generate as much as 100 times more angular dispersion than gratings and prisms, and they have been used to construct high-resolution spectrometers [13,14] and pulse shapers [15]. By the above Fourier-transform result, the huge angular dispersion of etalons implies that their output pulse front must be very tilted—by as much as 100 times that due to a diffraction grating. Indeed, that can be seen by simple light-travel-time considerations: the part of the pulse that makes the most passes through the etalon sees the most delay; and the thicker and more reflective the etalon, the more the dispersion and tilt.

Here we simulate and measure the complete spatiotemporal field of a ~ 700 ps, ~ 3 pm bandwidth pulse sent through an etalon. Because etalons are usually very lossy due to the highly reflective coating required on their entrance surface, we use an etalon with a small transparent gap on its entrance surface, which reduces the loss to essentially zero, and is usually referred to as a virtual image phase array (VIPA) [13] (see Fig. 2). For the simulations, we simply superimpose delayed and successively defocused replicas of the input pulse, where the number of replicas is chosen to produce the measured linewidth of the etalon.

Measuring the output pulse in space and time from the etalon is considerably more challenging, and—to our knowledge—such measurements have never been made. Even measuring the temporal field of our spatially uniform 700 ps directly out of the laser is quite difficult, requiring several nanoseconds of temporal range and/or picometer spectral resolution; and considering that diffraction gratings typically produce a maximum of 3 ps/mm of PFT (the grating size times the speed of light; see Fig. 1), the high finesse etalon can be expected to produce several *nanoseconds* of PFT across a 1 cm beam, corresponding to a tilt angle in excess of 89° , due to its increased angular dispersion, corresponding to a massively tilted pulse.

To accomplish this, we measure the spatio-spectral phase added to the pulse by the etalon using a linear interferometric frequency-domain technique used for measuring femtosecond and picosecond pulses, but extended to the nanosecond regime. We use the variation of spectral interferometry [16] usually known as crossed-beam spectral interferometry, which literally involves measuring a spectrally resolved spatial interferogram [17–20].

This requires a spectrometer with a spectral resolution equal to the inverse of the unknown pulse duration, or for our case <1 pm. Rather than using a very large and expensive diffraction-grating spectrometer to achieve the needed resolution, we use an etalon spectrometer. As a reference pulse, we use the beam directly from the laser, which is crossed with the tilted pulse out of the etalon at a small angle at a camera to produce spatial interference fringes. In the other dimension, we spectrally resolve the interference fringes using an etalon spectrometer so that a two-dimensional interferogram $I(x, \lambda)$ is measured. Using Fourier filtering along the x -dimension, the field of the tilted pulse, $E_{\text{unk}}(x, \lambda)$, is determined [19].

2. MODELING THE SPATIOTEMPORAL FIELD OF THE PULSE FROM AN ETALON

Intuitively we can estimate the PFT by considering that each delayed replica is also spatially shifted along the x direction due to the etalon’s tilt angle θ_{tilt} (see Fig. 2). So we expect the left side of the beam to be ahead in time compared to the right side by approximately $2dn/(c \cos \theta_{\text{tilt}})$ multiplied by the number of bounces of the beam inside the etalon. Considering that the number of bounces is approximately given by the finesse \mathfrak{F} , which we found experimentally to be 50 (see Section 3), for $d = 5$ mm, $n = 1.5$, and with $\theta_{\text{tilt}} = 1^\circ$, we expect 2.5 ns of the PFT across an output beam with a width along the x -dimension of ~ 5.8 mm.

To more precisely calculate the field emerging from the etalon shown in Fig. 2, for a given input pulse that is free of spatiotemporal couplings as well as temporal chirp, we

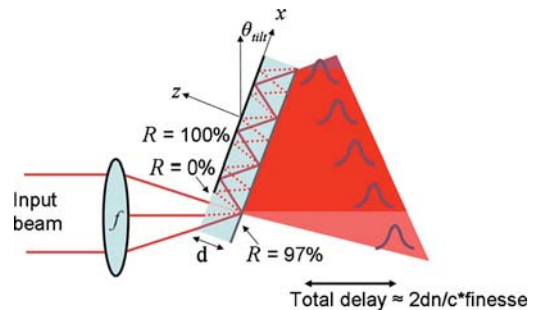


Fig. 2. (Color online) Schematic of an etalon, which yields PFT because each successive delayed pulse is laterally shifted in both space and time. The particular etalon shown here had a small uncoated gap at the bottom of the entrance face for more efficient insertion of the beam.

simply superimpose the emerging delayed, diverging, and transversely displaced replicas. We start with the field just after the lens $E_{\text{in}}(x, \lambda)$, which is given by

$$E_{\text{in}}(x, \omega, z=0) = \exp\left(-\left(\frac{\omega - \omega_0}{\Delta\omega}\right)^2 - \left(\frac{x}{w_0}\right)^2 - ikx \sin \theta_{\text{tilt}} + i\frac{k_0 x^2}{2f}\right), \quad (4)$$

where θ_{tilt} is the incident angle of the center ray at the etalon, w_0 is the input beam spot size, and $\Delta\omega$ is the spectral bandwidth. See Fig. 2 for the other parameters. The field immediately after the etalon is given by

$$E_{\text{out}}(x, \omega) = t_1 t_2 \sum_{m=0}^F (r_1 r_2)^m E_f(x, \omega, 2dm), \quad (5)$$

where t_1 , r_1 , t_2 , and r_2 are the reflection and transmission coefficients of the first and second surfaces of the etalon, and $E_f = E_{\text{in}}(x, \omega, z=f)$, that is, the field at the focus. To calculate the spatio-spectral field after each pass through the etalon, we use the angular-spectrum-of-plane-waves approach [21] to propagate the field from the previous pass by an additional distance of $2d$, as shown below:

$$E_f(x, \omega, 2dm) = \mathcal{J}_x^{-1}\{\mathcal{J}_x\{E_f(x, \omega, 2d(m-1))\} \times \exp(i2dnk_0\sqrt{1 - (k_x\lambda)^2})\}. \quad (6)$$

This involves a one-dimensional Fourier transform of the initial field to the k_x -domain, multiplying this field by the propagation kernel as a function of k_x , and then inverse-Fourier transforming back the x -domain. The same approach is used to propagate the initial field $E_{\text{in}}(x, \omega)$ up to the etalon's front surface to generate $E_f(x, \omega)$. The results of these simulations using our experimental parameters are shown in Section 4.

Note that, if the spectral range of the input pulse exceeds the free spectral range (FSR) of the etalon (given by $\lambda^2 \cos \theta / 2dn$), then multiple colors will emerge at the same angle, resulting in multiple overlapping pulse fronts, in which each pulse front will have a different tilt. Much as in the case of a diffraction grating, these multiple pulse fronts are the different orders. Our experiments produced 2–3 orders because, while the FSR (76 pm or 20 GHz for $d=5$ mm at 1064 nm) of the etalon was much greater than the pulse's bandwidth, focusing into it effectively increased the path length for the rays at larger angles, which also increased the FSR for these rays. In both our simulations and measurements we spatially filtered out the additional 2–3 orders that resulted in, and kept only the order containing the largest angular dispersion. Previous authors described a similar approach for modeling VIPA etalons, and they derived an analytical expression for the field at the focal plane of a lens placed after the etalon, which is useful for making a VIPA etalon spectrometer [22].

3. MEASURING THE SPATIOTEMPORAL FIELD OF THE PULSE FROM AN ETALON

A. Method

We use crossed-beam spectral interferometry to measure the spatiotemporal intensity and phase added to the in-

put pulse by the etalon (referred to as the PFT etalon) like that shown in Fig. 2. The back surface of the etalon was imaged onto a camera in the x or angular dispersion dimension of the PFT etalon, and in the other dimension, the beam was spectrally resolved with a second etalon spectrometer to achieve the needed spectral resolution. A spatially clean reference pulse crossed at a small angle with the tilted unknown pulse to produce the following interferogram at the camera:

$$I(x, \lambda) = |E_{\text{ref}}(\lambda)|^2 + |E_{\text{unk}}(x, \lambda)|^2 + |E_{\text{unk}}(x, \lambda)E_{\text{ref}}(\lambda)| \cos(kx\theta_c + \varphi_{\text{unk}}(x, \lambda) - \varphi_{\text{ref}}(\lambda)), \quad (7)$$

where θ_c is the crossing angle between the beams. The interferogram that we measured was the same as that measured in the method called Spatially Encoded Arrangement for Temporal Analysis by Dispersing a Pair of Light E-Fields (SEA TADPOLE) [18], except that the spatial information of the unknown pulse is simultaneously measured in our current measurements, because no fibers are used in our setup. Therefore we used an identical Fourier-filtering procedure to that used for the SEA TADPOLE to extract the spatio-spectral intensity and phase of the unknown pulse from the measured interferogram [18,19]. This process is illustrated in Fig. 3.

The top right image in Fig. 3 shows a typical interferogram that we measured. The fringes along the x -dimension are due to the beams' small crossing angle. Due to the angular dispersion in the beam from the etalon, the spatial fringe periodicity varies with wavelength. Similarly, for larger values of $|x|$, there are spectral fringes due to a delay between the reference and unknown pulses because of the tilt of the unknown pulse front.

B. Experimental Setup and Parameters

To measure the interferogram described above in order to characterize the tilted pulse out of an etalon, we use the experimental setup shown in Fig. 4. As our source we use a Standa Nd:LSB microdisk laser, which emits pulses centered at 1064 nm, with a repetition rate of 10 kHz and

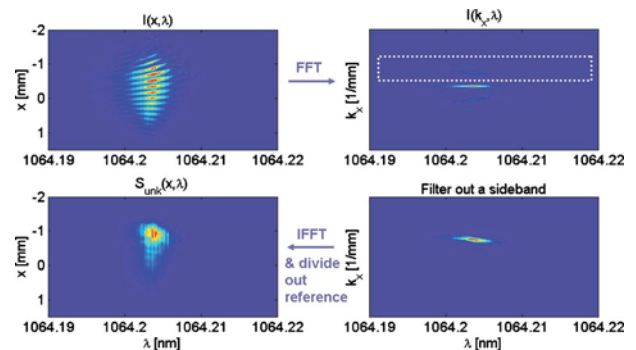


Fig. 3. (Color online) Retrieving the spatio-spectral field of the unknown pulse from the interferogram. The two-dimensional interferogram (top left) was Fourier transformed along the x -dimension. In the k_x -domain (top right) the data separated into three bands, where either the top or bottom band was isolated (bottom right) and then inverse-Fourier transformed back to the x -domain. The spatio-spectrum of the reference field was divided out from the resulting complex field to isolate the spatio-spectral intensity and phase of the pulse out of the etalon (bottom left). Only the intensities (indicated by color) are shown in the figure.

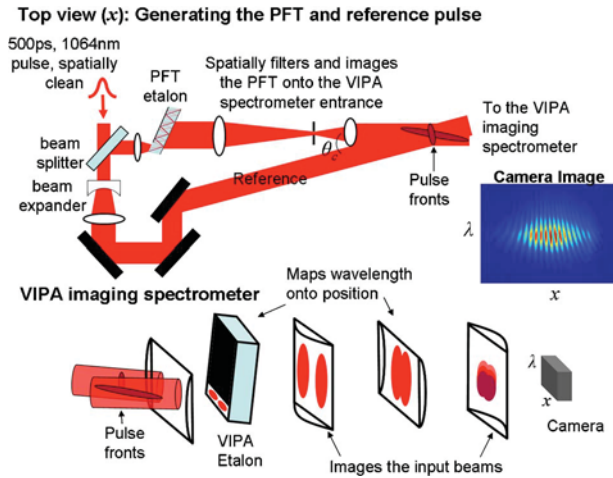


Fig. 4. (Color online) Experimental setup for measuring the spatiotemporal field of the pulse from an etalon. Top view: Along this dimension, the output of the laser was split into a reference and an unknown arm. In the unknown arm, the pulse was sent through the first etalon ($d=5$ mm), which introduced angular dispersion. The output of the PFT etalon was imaged onto the entrance of the etalon imaging spectrometer along the x -dimension. Also, in this dimension, the reference beam spatially overlapped and crossed at a small angle with the unknown pulse. In the etalon imaging spectrometer, the crossing beams were reimaged into the x -dimension of the camera resulting in vertical interference fringes. Along the camera's other dimension, the beams were spectrally resolved using an etalon to introduce angular dispersion and a cylindrical lens to map angle, or color, onto vertical position.

having a near-transform-limited duration of ~ 700 ps. To study the pulse after the etalon, we put a beam splitter at the output of the laser forming reference and unknown arms of the interferometer. The unknown beam passes through the first etalon (which we call the PFT etalon and with $d=5$ mm) adding the PFT. The pulse from the etalon propagated through a spatial filter, which removes the higher orders from the PFT etalon. This also demagnified the beam by $2\times$ and imaged it onto the entrance of the imaging spectrometer. Here the reference beam crossed at a small angle and spatially overlapped with the unknown beam. The imaging spectrometer imaged the crossing beams onto the camera's x -dimension, resulting in spatial interference fringes. Along the camera's other dimension, the crossing beams were spectrally resolved using a second wider etalon ($d=10$ mm) to generate angular dispersion, and then a cylindrical lens to map the angle or color onto position at the camera. This resulted in a two-dimensional interferogram at the camera. Note that, for flexibility, two lenses were used in the imaging spectrometer in order to achieve the desired demagnification of $2\times$.

The glass-spaced etalons for our experiments were custom made by CVI, and had a $>99.3\%$ reflectivity on the front surface and 97% reflectivity on the back surface, and a refractive index of 1.5 (ultraviolet fused silica) at 1064 nm. They were round with a diameter of 25.4 mm, and there was a small 3 mm uncoated gap in the front surface for inserting the beam. The PFT etalon had a FSR = 20 GHz, or 75 pm, and the second etalon for the spectrometer had a FSR of 10 GHz, or 38 pm. To determine the linewidths of each of these etalons, we used to them to spectrally resolve a wavelength-tunable New Focus Veloc-

ity laser, which had a much narrower linewidth than that of the etalons (<1 MHz). The widths of the measured spectra were found to be 0.9 pm (240 MHz) and 1.2 pm (320 MHz) for the 1 cm and 5 mm etalons, respectively. The etalon spectrometers were calibrated by scanning the frequency of this laser, or when this narrowband laser was not available, for the frequency-axis calibration, we used a Michelson interferometer to generate a double pulse from the Standa laser, which had a measurable (with a ruler) path-length difference, and therefore we knew the generated spectral-fringe spacing.

In the experimental setup shown in Fig. 4, the cylindrical lenses used to focus into the etalons both had focal lengths of 100 mm, and the lens in the spectrometer had a focal length of 500 mm. We estimated the etalon tilt angle with respect to the beam, θ_{tilt} , to be around 1° , and we found a value of 0.9° to produce simulations that fit best with what we measured. There was a total demagnification of $4\times$ of the beams at the camera: $2\times$ from the spatial filter and $2\times$ from the imaging lenses in the spectrometer. It was important to image the output of the etalon onto the camera; because, as a pulse containing angular dispersion propagates, spatial chirp is generated, reducing the PFT due to the decreased local bandwidth [3].

Note that in the above setup, and using the retrieval algorithm described in the previous section, we measured the spatio-spectrum and intensity added to the unknown pulse by the first etalon. Any phase terms that the unknown and reference pulses had in common, such as chirp in the laser output, canceled out in this measurement.

4. RESULTS AND DISCUSSION

Using the experimental setup described above, we measured the spatio-spectral field $E(x, \lambda)$ of the pulse just after the etalon. We knew the spectral line shape of the etalon in the spectrometer, so we first deconvolved it from the measured interferograms using MATLAB's built-in Richardson-Lucy algorithm. Then we retrieved the unknown pulse using the Fourier-filtering algorithm described above. We Fourier transformed the retrieved field to both the $k_x x$ and xt -domains to see both the angular dispersion and the PFT. The experimentally retrieved intensities in these three domains are shown at the top of Fig. 5. We also performed simulations using all of the experimental parameters described in Section 3 and the method described in Section 2. These results are shown at the bottom of Fig. 5.

As expected, the intensity $I(k_x, \lambda)$, which indicates the angular dispersion, shows a tilt, indicating that different colors are propagating at different angles (where $k_x = 2\pi/\lambda_0 \sin \theta$) due to the angular dispersion introduced by the etalon. By finding the maximum in the spectrum for each angle, we found the tilt to be linear and to have a slope of $3^\circ/\text{nm}$. Note that the angular dispersion is linear due to our small bandwidth and would not be if the pulse's bandwidth were a few hundred picometers or greater [22]. A diffraction grating with 1000 grooves/mm,

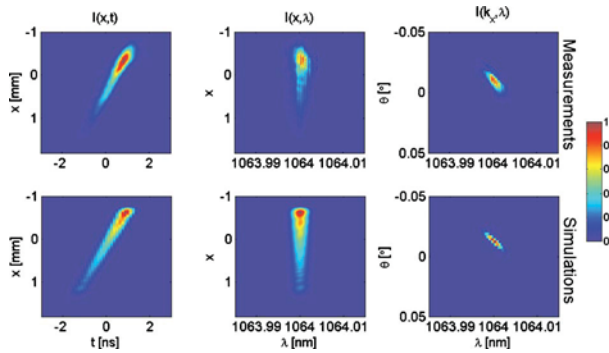


Fig. 5. (Color online) Experimental (top) and theoretical (bottom) results. Although both the spatio-spectral intensity and phase were measured, we instead show the intensity in three different domains, achieved by Fourier transforming the measured field. Center: The reconstructed intensity versus λ and x . No tilt was seen, indicating that there was no detectable spatial chirp. Left: Intensity versus x and t . A large PFT is apparent. Right: Intensity versus θ and λ , where $k_x = k_0 \sin \theta \approx 2\pi/\lambda \sin \theta$. The tilt is due to angular dispersion.

used at grazing incidence and for a wavelength of 1064 nm, results in an angular dispersion of $0.06^\circ/\text{nm}$, or about $1/50$ of that our PFT etalon. We also characterized the pulse's couplings with dimensionless ρ parameters, which are the normalized cross moments of the pulse's two-dimensional intensity, whose magnitudes are always ≤ 1 [23]. For the angular dispersion, we found that $\rho_{k\lambda} = 0.015$ for the pulse from the etalon, which was quite small due to the small bandwidth of our laser.

If angular dispersion is present, so is the PFT. This is apparent from the large tilt in the intensity $I(x,t)$ at the left in Fig. 5. Again, using curve fitting, we found the tilt to be linear and have a slope 1.3 ns/mm , or $\rho_{xt} = 0.27$, which is a large value for this parameter. The pulse out of the etalon is extremely tilted with its arrival time varying by 2.6 ns , or 78 cm , across the $\sim 2 \text{ mm}$ beam at the camera, that is, a tilt angle of 89.9° . As mentioned above, we used $4\times$ demagnification in the spatial filter and also in the simulations, so just after the etalon, the tilt would have been 325 ps/mm .

The spatio-spectrum $I(x,\lambda)$ shows no detectable tilt, and therefore no spatial chirp. The ρ parameter for this spectrum was $\rho_{x\lambda} = 0.006$, which is generally considered to be out of the detectable range or just due to noise in the data [23]. In the $x\lambda$ -domain, the coupling introduced by the etalon is known as *wave-front-tilt dispersion* [1], which is a phase coupling and which is why the spatio-spectral intensity in Fig. 5 is not tilted. A single Fourier transform moves a purely imaginary quantity into the intensity, which is why the coupling is apparent in the $k_x x$ and xt intensities as shown in Fig. 5.

The agreement between our simulations and measurements is good, with the main discrepancy being in our measured spatial profile. According to our simulations, the beam's spatial profile should approximately exponentially decay along the x -dimension because with each successive bounce in the etalon, the intensity is reduced by a factor of $r_1 r_2$. The spatial resolution in our measurements is limited by our ability to image the input beams through the spectrometer's etalon. This requires a large depth of field because each successive beam out of the etalon trav-

els an additional distance of $2dn$. Therefore, the depth of field needed is $2dn$ times the finesse, which is the propagation distance between the first and last passes of the etalon, or $\sim 60 \text{ cm}$ for our 10 mm etalon. Our imaging system consisted of a 30 cm followed by a 15 cm focal length cylindrical lens. Setting the depth of field equal to 60 cm , we find that the smallest possible feature that we could resolve at the camera is around 0.3 mm . Therefore the sharp edge of the spatiotemporal profile is smeared out in our measurements.

The other small discrepancy is in the width of the measured intensity $I(k_x, \lambda)$, which is likely due to the finite resolution of the etalon spectrometer. Even though we attempted to deconvolve its line shape from the measurements, its finite resolution cannot be perfectly accounted for. For example, the spectrometer's alignment may have been slightly different for our measurements than it was when we characterized the linewidth using a narrowband laser, perhaps due to the slight angle of the crossing beams.

5. CONCLUSIONS AND FUTURE WORK

Here we further illustrated the connection between angular dispersion and pulse-front tilt (PFT). We showed that the pulse emerging from an etalon exhibits a very large PFT: 2.6 ns across a 2 mm beam in our case, or 89.9° . We directly measured the spatiotemporal field of the pulse due to the etalon using crossed-beam spectral interferometry. In order to achieve the necessary spectral resolution to measure a pulse nanoseconds long, we constructed the interferometer using a second narrower-linewidth etalon to make an imaging etalon spectrometer. Our measurements also directly quantify the angular dispersion from the etalon, which we found to be 50 times more than the most that can be produced with a diffraction grating. Our results also confirm that the spatial chirp introduced by the etalon is negligible, and they are in reasonably good agreement with our simulations.

To our knowledge, these are the first spatiotemporal intensity-and-phase characterizations of a pulse in the nanosecond regime. Given that our etalon spectrometer has a finesse of 50 and a linewidth of 0.9 pm , we expect to be able to use it measure pulses with durations of 40 ps to $\sim 2 \text{ ns}$. However, because this method is linear, it can only detect spatiotemporal differences in the phase of the unknown pulse relative to the reference pulse. While this is useful for many cases, such as the measurements shown here, a self-referential method is needed to study the output of nanosecond lasers and amplifiers, and other non-linear effects of nanosecond pulses. We plan to address this problem in a future publication.

While angular dispersion is regularly exploited in applications, the PFT can be useful as well, because it maps pulse delay onto position. For example, the PFT could be used to make single-shot long-pulse frequency-resolved optical gating measurements or to perform any pump-probe experiment on a single shot. Our results illustrate that such ideas can be simply extended to allow for continuous nanosecond-range delays across a beam a mere centimeter wide.

ACKNOWLEDGMENTS

The authors acknowledge support from the Defense Advanced Research Projects Agency (DARPA) grant no. FA8650-09-C-9733 and help from Rick Toman of CVI Laser Corp. with the custom etalons. The views, opinions, and/or findings contained in this paper are those of the authors and should not be interpreted as representing the official views or policies, either expressed or implied, of the DARPA or the Department of Defense.

REFERENCES

1. S. Akturk, X. Gu, P. Gabolde, and R. Trebino, "The general theory of first-order spatio-temporal distortions of Gaussian pulses and beams," *Opt. Express* **13**, 8642–8661 (2005).
2. C. Dorrer, E. M. Kosik, and I. A. Walmsley, "Spatio-temporal characterization of the electric field of ultrashort optical pulses using two-dimensional shearing interferometry," *Appl. Phys. B* **74**, 209–217 (2002).
3. Z. Bor, B. Racz, G. Szabo, M. Hilbert, and H. A. Hazim, "Femtosecond pulse front tilt caused by angular dispersion," *Opt. Eng. (Bellingham)* **32**, 2501–2504 (1993).
4. J. Hebling, "Derivation of the pulse front tilt caused by angular dispersion," *Opt. Quantum Electron.* **28**, 1759–1763 (1996).
5. O. E. Martinez, "Pulse distortions in tilted pulse schemes for ultrashort pulses," *Opt. Commun.* **59**, 229–232 (1986).
6. O. E. Martinez, "Grating and prism compressors in the case of finite beam size," *J. Opt. Soc. Am. B* **3**, 929–934 (1986).
7. S. Akturk, X. Gu, E. Zeek, and R. Trebino, "Pulse-front tilt caused by spatial and temporal chirp," *Opt. Express* **12**, 4399–4410 (2004).
8. R. Wyatt and E. E. Marinero, "Versatile single-shot background-free pulse duration measurement technique for pulses of subnanosecond to picosecond duration," *Appl. Phys.* **25**, 297–301 (1981).
9. G. Szabó, Z. Bor, and A. Müller, "Phase-sensitive single-pulse autocorrelator for ultrashort laser pulses," *Opt. Lett.* **13**, 746–748 (1988).
10. W. Yang, P. G. Kazansky, and Y. P. Svirko, "Non-reciprocal ultrafast laser writing," *Nat. Photonics* **2**, 99–104 (2008).
11. S. Xiao, J. D. McKinney, and A. M. Weiner, "Photonic microwave arbitrary waveform generation using a virtually imaged phased-array (VIPA) direct space-to-time pulse shaper," *IEEE Photon. Technol. Lett.* **16**, 1936–1938 (2004).
12. M. Born and E. Wolf, *Principles of Optics*, 7th ed. (Cambridge University Press, 1999).
13. M. Shirasaki, "Large angular dispersion by a virtually imaged phased array and its application to a wavelength demultiplexer," *Opt. Lett.* **21**, 366–368 (1996).
14. S. Xiao and A. Weiner, "2-D wavelength demultiplexer with potential for 1000 channels in the C-band," *Opt. Express* **12**, 2895–2902 (2004).
15. V. R. Supradeepa, C. B. Huang, D. E. Leaird, and A. M. Weiner, "Femtosecond pulse shaping in two dimensions: Towards higher complexity optical waveforms," *Opt. Express* **16**, 11878–11887 (2008).
16. C. Froehly, A. Lacourt, and J. C. Vienot, "Time impulse response and time frequency response of optical pupils," *Nouv. Rev. Opt.* **4**, 183–196 (1973).
17. D. Meshulach, D. Yelin, and Y. Silberberg, "Real-time spatial-spectral interference measurements of ultrashort optical pulses," *J. Opt. Soc. Am. B* **14**, 2095–2098 (1997).
18. P. Bowlan, P. Gabolde, A. Schreenath, K. McGresham, R. Trebino, and S. Akturk, "Crossed-beam spectral interferometry: a simple, high-spectral-resolution method for completely characterizing complex ultrashort pulses in real time," *Opt. Express* **14**, 11892–11900 (2006).
19. J. P. Geindre, P. Audebert, S. Rebibo, and J. C. Gauthier, "Single-shot spectral interferometry with chirped pulses," *Opt. Lett.* **26**, 1612–1614 (2001).
20. K. Misawa and T. Kobayashi, "Femtosecond Sangac interferometer for phase spectroscopy," *Opt. Lett.* **20**, 1550–1552 (1995).
21. J. W. Goodman, *Introduction to Fourier Optics* (Roberts, 2005).
22. S. Xiao, A. M. Weiner, and C. Lin, "A dispersion law for virtually imaged phased-array spectral dispersers based on paraxial wave theory," *IEEE J. Quantum Electron.* **40**, 420–426 (2004).
23. P. Gabolde, D. Lee, S. Akturk, and R. Trebino, "Describing first-order spatio-temporal distortions in ultrashort pulses using normalized parameters," *Opt. Express* **15**, 242–251 (2007).